Time-of-flight patterns of ultra-cold bosons in optical lattices in various Abelian artificial magnetic field gauges

T. P. Polak
Faculty of Physics, Adam Mickiewicz University of Poznań, Umultowska 85, 61-614 Poznań, Poland

T. A. Zaleski
Institute of Low Temperature and Structure Research, Polish Academy of Sciences, Okólna 2, 50-422 Wrocław, Poland

We calculate the time-of-flight patterns of strongly interacting bosons confined in two-dimensional square lattice in the presence of an artificial magnetic field using quantum rotor model that is inherently combined with the Bogolyubov approach. We consider various geometries of the magnetic flux, which are expected to be realizable, or have already been implemented in experimental settings. The flexibility of the method let us to study cases of the artificial magnetic field being uniform, staggered or forming a checkerboard configuration. Effects of additional temporal modulation of the optical potential that results from application of Raman lasers driving particle transitions between lattice sites are also included. The presented time-of-flight patterns may serve as a verification of chosen gauge in experiments, but also provide important hints on unconventional, non-zero momentum condensates, or possibility of observing graphene-like physics resulting from occurrence of Dirac cones in artificial magnetic fields in systems of ultra-cold bosons in optical lattices. Also, we elucidate on differences between effects of magnetic field in solids and the artificial magnetic field in optical lattices, which can be controlled on much higher level leading to effects not possible in condensed matter physics.

PACS numbers: 67.85.Hj, 03.75.K.k, 05.30.Jp

I. INTRODUCTION

The experimental observation of Bose Einstein condensation [1] of trapped atomic gases catalyzed a very large further research activity in studies of behavior of atoms obeying Bose-Einstein statistics. This led to loading of ultra-cold bosonic atoms into optical lattices, which offer a clean setting for quantitative and highly precise investigations of quantum phase transitions in the strongly interacting atomic systems [2]. The behavior of the atoms bears resemblance to the physics of strongly-correlated electronic systems like high-T_c superconductors, which are described by similar microscopic Hamiltonians (Hubbard model) [3]. Although the particles that are loaded to optical lattices are electrically neutral, it is possible to impose additional external potential, which forces them to behave exactly like charged particles interacting with an external magnetic field. In the simplest case the potential can result from rotation, following from formal equivalence between the Lorentz force and the Coriolis force [4, 5]. However, more control is obtained using additional photon-assisted tunneling to coherently transfer atoms from one internal state to another. This induces a non-vanishing phase of particles moving along a closed path, which simulates magnetic flux through the lattice [5–8]. Such techniques are under very active investigation. Since, quantum optics technology provides unprecedented degree of manipulation of structure of such imposed magnetic flux, it allows for obtaining very strong magnetic fields for neutral atoms: both Abelian [9, 10] and non-Abelian [11, 12]. A long-term goal of these experiments is to achieve the quantum Hall regime, in which very high value of effective flux opens an avenue to study the effects that are not achievable in the conventional solid state physics [13, 14].

The dynamic properties of the trapped ultra-cold atoms can be investigated in time-of-flight (TOF) experiments, in which the trapping potential is suddenly switched off. As the atoms are no longer being localized spatially, their scattering ratio decreases and the momentum distribution becomes temporarily frozen, with gravity being the only force acting on the atomic cloud. The infra-red absorption images taken after arbitrary expansion time show locations of the atoms, which are directly related to the the distribution of the momenta $n(\boldsymbol{k})$ in the system before the potential was switched off. In the superfluid state (SF) the TOF images exhibit characteristic sharp maxima related to long-range phase coherence of the condensate. While the phase fluctuations are being increased by stronger interactions between atoms, the sharp features disappear and $n(\mathbf{k})$ becomes a wide maximum indicating the presence of the Mott insulating (MI) state [2].

Theoretical challenge in describing the TOF patterns results from the dynamic nature of the problem: determination of the momentum distribution $n(\mathbf{k})$ requires precise knowledge of spatial correlations between atoms, namely atom-atom correlation function. This precludes use of methods based on mean-field approximation. In the present paper we apply a recently proposed combination of quantum rotor (QR) approach and Bogolyubov method, which has been successfully applied to investigate correlations in systems of cold atoms in optical lattices (e.g. time-of-flight patterns [15], spectral functions

[16]). It is also a natural extension of the QR model that was used to describe the phase diagram, also in the presence of the artificial magnetic field [17–19]. The QR approach has been verified [20, 21] using other methods, like Monte Carlo numerical calculations [22] and diagrammatic perturbation theory [23]. The QR phase diagrams were also analyzed in the context of an analytical works: mean-field theory [24] and Padé analysis [25].

It is our goal to calculate the TOF patterns for various gauges of the magnetic field that are expected to be realizable or have already been implemented in the experimental settings to investigate the dynamics of the condensate and the phase transition to the localized state. The remainder of the paper is as follows: in. Sec II we introduce the model Hamiltonian relevant to strongly correlated bosons confined in two-dimensional square lattice. Then we apply the synthetic magnetic field**,** which modifies the hopping term in the Hamiltonian and add additional temporal modulation of the optical potential. The main points of our approach that lead to calculation of the atom-atom correlation function are summarized in Sec. III. Furthermore, we present the time-of-flight patterns in the following Section. Our results are summarized in Sec. V, while the dispersion relations and the resulting lattice densities of states used in calculations are presented in Appendix.

II. MODEL HAMILTONIAN

The essential physics of bosons in optical lattice can be captured using the single-band Bose-Hubbard model. In this description, the particles move within a tight-binding scheme and interact only through on-site repulsion resulting from interatomic collisions (since the atoms are neutral). The Hamiltonian is given by,

$$\mathcal{H} = -\sum_{\langle i,j\rangle} t_{ij}\left(b_i^\dagger b_j + b_j^\dagger b_i\right) + \frac{U}{2}\sum_i n_i\left(n_i-1\right) - \mu\sum_i n_i, \tag{1}$$

where $b_i\left(b_i^\dagger\right)$ is the boson destruction (creation) operator at a site i, $n_i = b_i^\dagger b_i$ is the density operator, $U>0$ is the on-site repulsion and μ is the chemical potential, which controls the number of bosons. Here, $\langle i,j\rangle$ denotes summation over the nearest-neighbor sites. Finally, t_{ij} is the hopping matrix element, which is non-zero only for the nearest neighbors and equal to t. For any given lattice geometry and depth, both t and U can be calculated directly by finding the respective Wannier function basis [26]. Introduction of the synthetic magnetic field $\mathbf{B}$ (potential that acts on neutral particles in the same fashion as the magnetic field acts on charges, e.g. rotation of the system, laser stirring, selective driving of hopping with Raman lasers) leads to introduction of the Peierls phase factor:

$$\exp\left(\frac{2\pi i}{\Phi_0}\int_{\mathbf{r}_i}^{\mathbf{r}_j}\mathbf{A}\cdot d\mathbf{l}\right), \tag{2}$$

which is a consequence of the gauge invariance of the Schrödinger equation, where $\mathbf{B} = \nabla\times\mathbf{A}\left(\boldsymbol{r}\right)$ and $\Phi_0 = h/e$ is the flux quantum, with $\mathbf{A}\left(\boldsymbol{r}\right)$ being the vector potential. This leads to modification of the hopping term:

$$-\sum_{\langle i,j\rangle} t_{ij}\left(b_i^\dagger b_j + b_i b_j^\dagger\right) \rightarrow -\sum_{\langle i,j\rangle} t_{ij}\left(b_i^\dagger b_j e^{\frac{2\pi i}{\Phi_0}\int_{\mathbf{r}_i}^{\mathbf{r}_j}\mathbf{A}\cdot d\mathbf{l}} + b_i b_j^\dagger e^{-\frac{2\pi i}{\Phi_0}\int_{\mathbf{r}_i}^{\mathbf{r}_j}\mathbf{A}\cdot d\mathbf{l}}\right). \tag{3}$$

that as a result, instead of being a real value, becomes a complex number:

$$t_{ij}\rightarrow t_{ij}^{'} \equiv t_{ij}e^{\frac{2\pi i}{\Phi_0}\int_{\mathbf{r}_i}^{\mathbf{r}_j}\mathbf{A}\cdot d\mathbf{l}}. \tag{4}$$

Furthermore, particles hopping along closed loops of the lattice cell (area a) gain an additional phase $\phi\equiv 2\pi f$ imposed by the external uniform synthetic magnetic field potential, where $f = aBe/2\pi\hbar$. We also permit for additional spatial modification of the on-site potential $(-1)^i\Delta$, which allows us to describe the effect of temporal modulation by the photon-assisted tunneling that are used to drive the phase change in some experiments. The range of actual gauges (shapes of the vector potential $\mathbf{A}$) applied to the system, which can be realized experimentally, is very wide (see, Sec. IV). The change of the hopping parameter in Eq. (4) also modifies the band structure, which becomes very complex. Complicated multi-band dispersion relations provide difficulties in calculating analytical formulas in the uniform case for the lattice density of states (DOS) limiting availability to a few selected values of f [17].

III. CORRELATION FUNCTIONS

In optical lattices, the phase transition between superfluid and Mott insulator states occurs in the regime of intermediate to strong interactions ($U\gg t$). As a result, a theory that goes beyond standard Bogoliubov approximation is required. To this end, we calculate the one-particle correlation function that is necessary to predict the time-of-flight patterns using the quantum rotor approach (see, Ref. [19]) combined with the Bogolyubov method that has been recently proposed and succesfully applied to systems of bosons in optical lattices [15]. This scenario provides a picture of quasiparticles and energy excitations in the strong interaction limit, where the transition between the superfluid and the Mott state is driven by phase fluctuations. The approach is based on separation of the problem into the amplitude of the Bose field and the fluctuating phase that was absent in the original Bogoliubov problem. As a results, one arrives at a formalism, where the one-particle correlation functions are treated self-consistently and permit us to investigate a whole range of phenomena described by the Bose-Hubbard Hamiltonian. Furthermore, the phase fluctuations are described within the quantum spherical model

[27], which goes beyond mean-field approximation including both quantum and spatial correlations. Although, the approach easily allows for non-zero temperatures, in the following we restrict ourselves to the description of the ground state of the system ($T = 0$). As the details of calculations have been extensively presented in Ref. [15], we only summarize the main steps of the approach here. We start by introducing the functional integral representation of the model in Eq. (1) in terms of the the complex fields $a_i(\tau)$, which leads to the partition function:

$$\mathcal{Z} = \int [\mathcal{D}\bar{a}\mathcal{D}a]\, e^{-\mathcal{S}[\bar{a},a]} \tag{5}$$

with the action $\mathcal{S}$ given by

$$\mathcal{S}[\bar{a},a] = \sum_i \int_0^\beta d\tau \left[\bar{a}_i(\tau)\frac{\partial}{\partial\tau}a_i(\tau) + \mathcal{H}(\tau)\right], \tag{6}$$

where $\beta = 1/k_{\mathrm{B}}T$ and T being temperature. Next, we perform the local gauge transformation to the new bosonic variables

$$a_i(\tau) = b_i(\tau)\exp\left[i\varphi_i(\tau)\right]. \tag{7}$$

It allows to extract phase variable $\varphi_i(\tau)$, which ordering naturally describes the superfluid – Mott insulator transition, and the amplitude $b_i(\tau)$ that is related to the superfluid density. As a result, the the partition function becomes:

$$\mathcal{Z} = \int \left[\mathcal{D}\bar{b}\mathcal{D}b\right]\left[\mathcal{D}\varphi\right] e^{-\mathcal{S}\left[\bar{b},b,\varphi\right]}, \tag{8}$$

with the action $\mathcal{S}\left[\bar{b},b,\varphi\right] \equiv S\left[\bar{a},a\right]$. The statistical sum in Eq. (8) can be integrated over the phase or amplitude variables leading to phase-only of amplitude-only actions:

$$\begin{aligned}\mathcal{S}_\varphi[\varphi] &= -\ln\int[\mathcal{D}\varphi]\, e^{-\mathcal{S}[\varphi]},\\ \mathcal{S}_b\left[\bar{b},b\right] &= -\ln\int\left[\mathcal{D}\bar{b}\mathcal{D}b\right] e^{-\mathcal{S}\left[\bar{b},b\right]},\end{aligned} \tag{9}$$

to obtain:

$$Z = \int[\mathcal{D}\varphi]\, e^{-\mathcal{S}_\varphi[\varphi]} = \int\left[\mathcal{D}\bar{b}\mathcal{D}b\right] e^{-\mathcal{S}_b\left[\bar{b},b\right]}. \tag{10}$$

The main point of the approach is the calculation of the action $\mathcal{S}_\varphi[\varphi]$ in Eq. (9), which describes the phase-only model with amplitudes integrated out. It is subsequently mapped onto the quantum spherical model, which can be solved analytically.

As a result of the variable transformation in Eq. (7), the superfluid order parameter, which non-vanishing value signals a macroscopic quantum phase coherence (identified as the superfluid state), factorizes:

$$\Psi_B \equiv \langle a_i(\tau)\rangle_a = \langle b_i(\tau)\rangle_b \langle\exp\left[i\varphi_i(\tau)\right]\rangle_\varphi. \tag{11}$$

This reflects the fact that all atoms in the condensate form a coherent matter wave having the same phase. The averages in Eq. (11) are defined as:

$$\langle\ldots\rangle_x = \frac{\int[\mathcal{D}x]\ldots e^{-\mathcal{S}_x[x]}}{\int[\mathcal{D}x]\, e^{-\mathcal{S}_x[x]}} \tag{12}$$

for $x = a,\, b,\, \varphi$ and the respective actions: $\mathcal{S}\left[\bar{a},a\right]$, $\mathcal{S}\left[\bar{b},b\right]$ or $\mathcal{S}_\varphi[\varphi]$. Furthermore, we parametrize the boson fields

$$b_i(\tau) = b_0 + b_i'(\tau), \tag{13}$$

where $b_0 = \sqrt{N_0}$ is the Bose condensate macroscopic occupation and $b_i'(\tau)$ is the amplitude fluctuation around the mean value b_0. As a result, the superfluid order parameter becomes:

$$\Psi_B = b_0 m_0, \tag{14}$$

where m_0 is phase order parameter:

$$m_0 = \langle\exp\left[i\varphi_i(\tau)\right]\rangle. \tag{15}$$

The atom-atom correlation function

$$C_{ij}(\tau) = \langle a_i(\tau)\,\bar{a}_j(\tau)\rangle_x \tag{16}$$

also factorizes due to the variable transformation in Eq. (7) becoming:

$$C_{ij}(\tau) = \left\langle b_i\bar{b}_j\right\rangle_b \langle\exp\left[\varphi_i(\tau) - \varphi_j(\tau)\right]\rangle_\varphi \tag{17}$$

with the averages that can be calculated analytically for any lattice, for which the dispersion relation $t_{\mathbf{k}}$ (Fourier transform of the hopping t_{ij}) is known [15]. The momentum distribution of the atoms in optical lattice is then a Fourier transform of the correlation function:

$$n(\mathbf{k}) = \int_0^\beta d\tau \sum_{\boldsymbol{R}=|\boldsymbol{r}_i-\mathbf{r}_j|} C_{ij}(\tau)\, e^{i\mathbf{k}\mathbf{R}}. \tag{18}$$

This leads to the density of particles in the time-of-flight experiments [15, 28]:

$$n(\mathbf{r}) = \left(\frac{m}{\hbar t_e}\right)^3 \left|W\left(\mathbf{k} = \frac{m}{\hbar t_e}\mathbf{r}\right)\right|^2 n\left(\mathbf{k} = \frac{m}{\hbar t_e}\mathbf{r}\right), \tag{19}$$

where $|W(\mathbf{k})|$ is the envelope of the Fourier transform of the Wannier function for the chosen optical lattice and t_e is the expansion time. It should be pointed out that the envelope $|W(\mathbf{k})|$ can in principle depend not only on the optical lattice potential, but also on the presence of the artificial magnetic field [29]. However, since its calculation goes beyond the scope of the present work, we use the standard form:

$$\left|W\left(\frac{m\mathbf{r}^2}{\hbar t_e}\right)\right|^2 \approx \frac{1}{\pi^{3/2}w_t}\exp\left(-\frac{\mathbf{r}^2}{w_t^2}\right), \tag{20}$$

where $w_t = \hbar t_e/mw_0$ with w_0 being the size of the on-site Wannier function [15]. This choice can be justified by comparing the resulting TOF patterns with experimental ones [10] and observing the conformity of the particle density decays as a function of $\mathbf{r}$ in both cases (see, Sec. IV D).

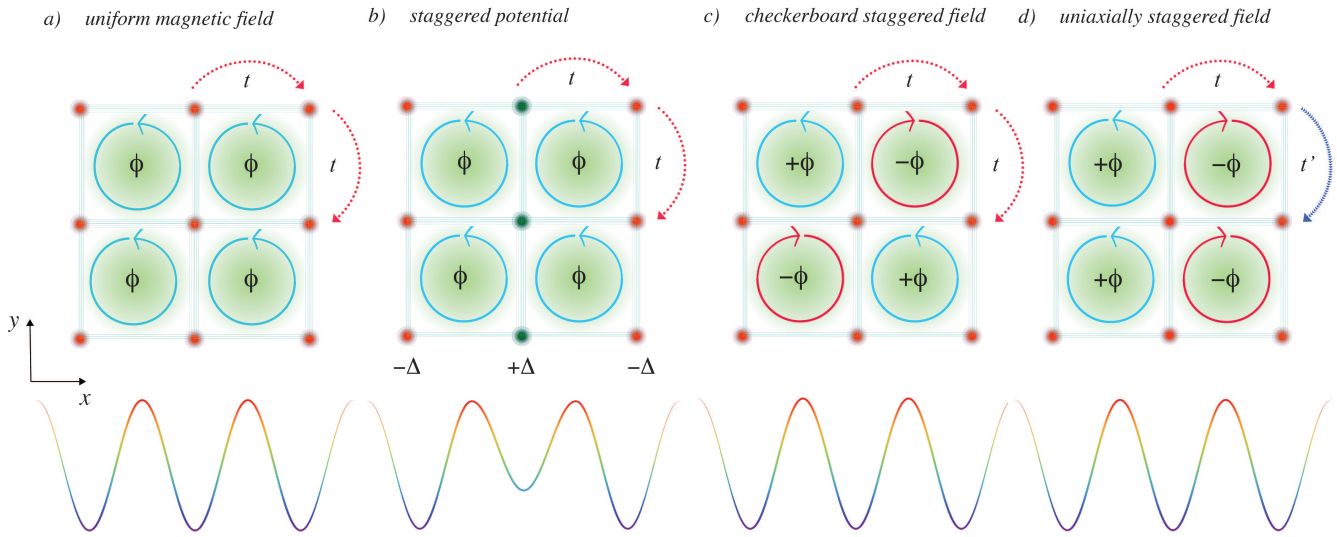

Figure 1: (Color online) Geometry of the artificial magnetic field in various gauges resulting in different flux configuration: a) uniform, b) uniform with additional staggered potential, c) staggered flux with checkerboard arrangement, d) uniaxially staggered flux. Value of the flux per plaquette being the phase acquired by a particle traveling around an elementary cell is ϕ. Additional staggering on-site potential is denoted by $\pm\Delta$.

IV. EXPERIMENTAL GAUGES OF THE SYNTHETIC MAGNETIC FIELD

The momentum distribution is an important observable since it allows to identify whether the atoms in the optical lattice are in the superfluid or Mott insulating state. Although, the existence of sharp peaks in the time-of-flight images that used to be unequivocally associated with the emergence of the superfluidity is not believed to be sufficient criterion [28], recent analysis have shown that the momentum distribution can be used to make pretty accurate estimations about location of the critical regime [30].

In the following, we calculate the time-of-flight patterns resulting from Eq. (19) for various gauges of the artificial magnetic field. We start from determining the dispersion relation $t_{\mathbf{k}}$ for the chosen gauge, which allows us to obtain the atom-atom correlation function in Eq. (17) by using the procedure described in details in Ref. [15].

We present all the results along similar scheme: first we plot $t_{\mathbf{k}}$ for the chosen gauge and then the calculated time-of-flight patterns in the superfluid state, near the SF-MI phase transition and in the Mott insulator. We measure the interaction strength between atoms using the experimental quantities V_0 and E_R instead of t and U, where V_0 is the optical potential depth and E_R – the recoil energy. The relation of V_0/E_R to t/U is presented in Ref. [15]. One should also note that the minimum of kinetic energy in the Hamiltonian in Eq. (1) corresponds to the maximum of $t_{\mathbf{k}}$ due to the minus sign in the hopping term.

A. Uniform magnetic field

We start with the uniform artificial magnetic field, which acts on atoms in optical lattices in identical way as a homogeneous magnetic fields acts on electrons in solids (see, Fig. 1a). Every elementary cell of the lattice is pierced by a fraction f of the elementary flux, which leads to additional phase ϕ acquired by a particle moving around the cell equal to $\phi \equiv 2\pi f$. Such a configuration of the artificial magnetic field can be realized using various gauges, e.g. Landau $\mathbf{A} = B\,(0, y, 0)$, or symmetric $\mathbf{A} = \frac{B}{2}\,(-y, x, 0)$. This results in increase of the elementary cell, since translational symmetry is locally broken for non-integer values of f. If f is a rational, being equal to $f = p/q$, the cell enlarges q-fold, while the Brillouin zones shrinks by the same factor (leading to so-called magnetic Brillouin zone). The quasiparticle spectrum has a complicated multi-band structure known as the Hofstadter butterfly [14] (the denominator q determines the number of sub-bands) and can be generated using Harper's equation [13]. Although, the general solution is unknown, for special values of f equal to $f = 1/2, 1/3, 1/4, 1/6, 1/8, 3/8$ both dispersion relation and lattice density of states have been analytically calculated [21]. We see, that the denominator of the expression describing the magnetic field $f = p/q$ determines the number of bands.

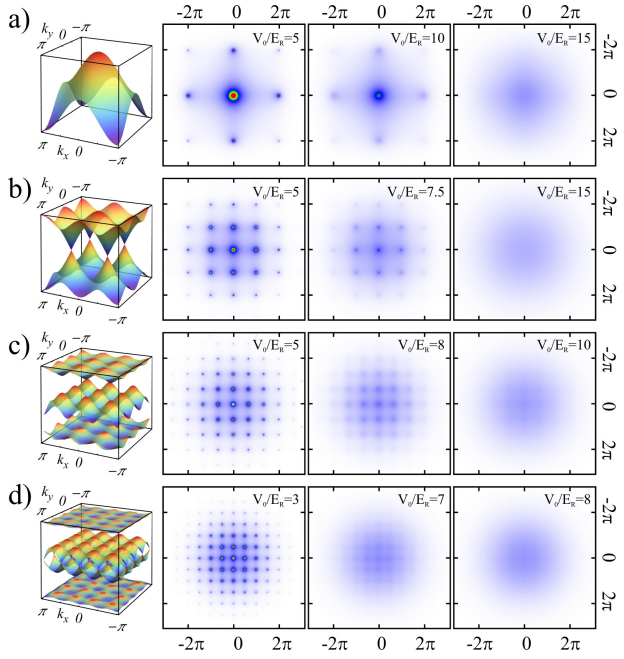

Figure 2: (Color online) Dispersion relation and time-of-flight patterns for atoms in optical lattice without (a) and under uniform artificial magnetic field: b) $f = 1/2$, c) $f = 1/3$, d) $f = 1/4$. The TOF images depict superfluid state (the first column), system close to the phase transition (the second column) and the Mott insulator (the last column).

The dispersion relations for $f = 0$, $1/2$, $1/3$ and $1/4$ have been presented in Fig. 2 along with the resulting TOF patterns. In the superfluid state, the spectrum has sharp coherence peaks, which slowly fade away, when the system is driven towards the phase transition. Finally, in the Mott insulator, the TOF patterns become a wide, feature-less maximum with no signatures of the phase coherence. The most notable influence of the synthetic magnetic field is a change in periodicity leading to shrinking of the Brillouin zone and accompanying dense packing of the coherence peaks in the SF state. As a result, small fluxes could be difficult to detect. In the typical TOF experiment the $2\hbar k$ of the Brillouin zone corresponds to the 50 pixels on the charge-coupled-device (CCD) camera. The smallest detectable separation between two momentum peaks is around 10 pixels which matches the $1/5$ of the Brillouin zone, therefore the fluxes below $\phi < 2\pi/5$ ($f = 1/5$) will be hardly recognizable from the experimental data. Moreover, the key role is the proper preparation of the ground state, in which the coherence over large area of the real space is obtained to avoid further peaks broadening [31]. In the theoretical calculations the resolution of the TOF diagrams can be in principle arbitrarily high and two peaks will become indistinguishable when the distance between them becomes of the order of the full width at half maximum of the $n(\boldsymbol{k})$ peaks, which in this case is about 3.5% of the first Brillouin zone width.

1. $f = 1/2$ ($\phi = \pi$)

Since, the single-particle spectrum is symmetric around $f = 1/2$: $t_{\mathbf{k}}(f) \equiv t_{\mathbf{k}}(1-f)$, the strongest possible uniform artificial magnetic field that can be achieved is $f = 1/2$, which results in flux $\phi = \pi$ per plaquette. In this case $t_{\mathbf{k}}$ has two sub-bands, which meet at $t_{\mathbf{k}_D} = 0$ forming Dirac cones (the spectrum is linear near $\mathbf{k}_D$ and rotationally symmetric: $t_{\mathbf{k}} \sim |\mathbf{k} - \mathbf{k}_D|$). This leads to potential possibility of observing graphene-like physics in optical lattices. The time-of-flight patterns for $f = 1/2$ are presented in Fig. 3. In the case when bosons are free to occupy any of the sub-bands (see, Fig. 3a), the TOF images show coherence peaks in the superfluid state at the momenta, for which the kinetic energy assumes minimal values ($\mathbf{k} = \{n\pi, m\pi\}$,where n, m are integers, which are basically $\mathbf{k} = 0$ point repeated by periodicity of the reciprocal lattice). The $\mathbf{k}_D$ points corresponding to intersections of the bands do not show in the TOF patterns. However, if *all* particles were occupying *only* the upper band, the kinetic energy minima would appear at $\mathbf{k}_D$, which has been presented in Fig. 3b. The resulting superfluid state exhibits non-zero momentum, with $\mathbf{k} = 0$ component totally removed. On the other hand, in case of populating the lower band only (see, Fig. 3c), the resulting picture does not differ much from the scenario, when occupation of both bands is allowed (in Fig. 3a), however some slight differences are noticeable. It results from the fact that although we are investigating the ground state of the system, not all bosons occupy the lowest energy state. Since the particles are interacting, only a fraction of them contributes to the condensate (thus occupies the lowest energy state), while the rest can be driven to higher energy states by the quantum fluctuations, which are present even in zero temperature. This also leads to a conclusion that in systems of bosons the properties of the superfluid state are determined by the points in the k-space around the minima of the kinetic energy. However, in the vicinity of the SF-MI phase transition the sharp maxima are gone, and the TOF images depict momentum distribution of the incoherent particles. Surprisingly, they contain weak maxima around $\mathbf{k} = 0$ points regardless of location of the superfluid peaks.

In order to observe effects resulting from existence of the Dirac cones in the excitation spectra, population of the respective bands has to be engineered. It can be experimentally realized using projection of the condensates onto a desired Bloch state [32]: the system of bosons, which initially is in the superfluid phase, is released from the trap and expands freely for a short period of time. Then, a moving optical lattice is introduced, which is created by laser beams with additional acousto-optic modulators that allow for shifting positions of the lattice minima. As a result, depending on the modulation, the BEC can be loaded to a lattice state with an arbitrary and well-defined quasi-momentum. Using this approach, it was possible to access different energy bands of the ^{87}Rb

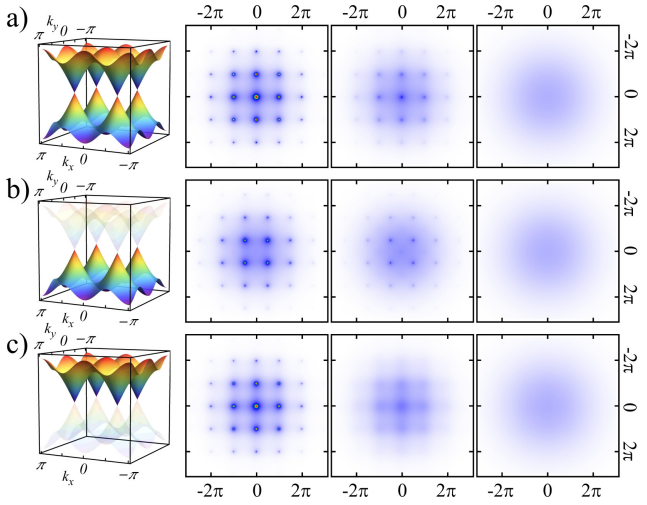

Figure 3: (Color online) Dispersion relation and time-of-flight patterns for atoms in optical lattice under uniform artificial magnetic field $f = 1/2$: a) both sub-bands filled, b) higher sub-band filled, c) lower sub-band filled. The TOF images depict superfluid state (the first column, $V_0/E_R = 5$), system close to the phase transition (the second column, $V_0/E_R = 7.5$) and the Mott insulator (the last column, $V_0/E_R = 15$).

atoms allowing a high precision studies of the lensing effect on a Bose-Einstein condensate [33].

It should be also noted that the appearance of the Dirac intersections in the Hofstadter spectra occurs for magnetic fields $f = p/q$, for which q is even and is never observed for odd values Fig. 2.

B. Uniaxial staggered potential

Application of the additional staggering potential $\Delta/2t \equiv \tilde{\Delta}$ that drives hopping of atoms between chosen lattice sites [see Sec. II] is a natural extension of the system in the uniform magnetic fields (see, Fig. 1b). It allows to manipulate the Dirac cones: change the distance between them in the k-space and annihilate them when two of them merge [34]. For $f = 1/2$ (flux through the elementary cell $\phi = \pi$) and $\tilde{\Delta} = 0$, the system is identical to described in Sec. IV A 1 and the resulting TOF patterns are presented in Fig. 4a. While the $\tilde{\Delta}$ is being increased, the Dirac points move closer to each other (see, Fig. 4b-c) and for $\tilde{\Delta} = 1$ – merge. For $\tilde{\Delta} > 0$, the Dirac points annihilate and the single-particle spectrum becomes gapped (Fig. 4d-e). However, as in the previous case of the uniform field, if both sub-bands are populated, the condensation of bosons occurs around the bottom of the lower band, thus Dirac cones have no effect on the TOF patterns. On the other hand, increasing value of $\tilde{\Delta}$ strongly enhances hopping along one direction leading to slow decline in weight of $\mathbf{k} = 0$ maximum, enlarging $(n\pi, \pm\pi)$ components (with $n \neq 0$). This effect can be reversed by enlarging interatomic interactions (U/t): near

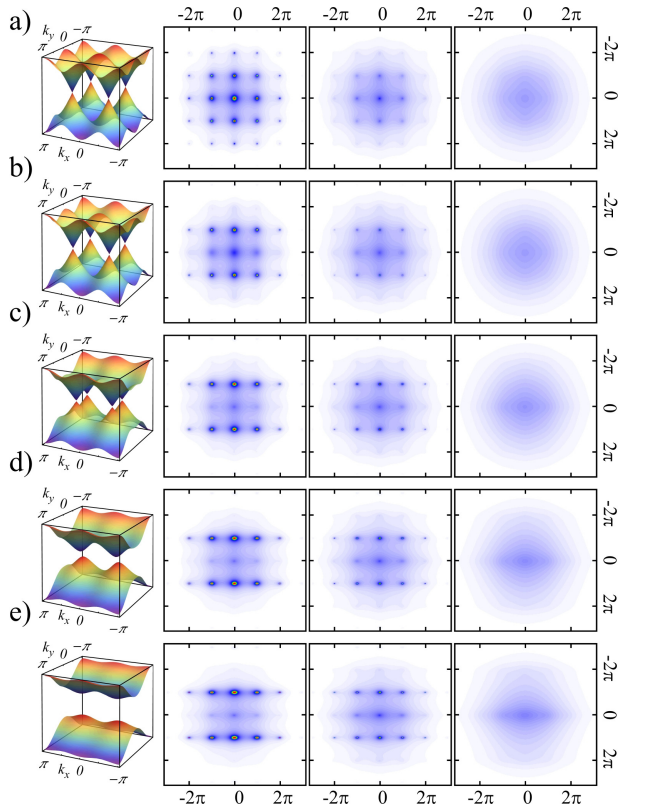

Figure 4: (Color online) Dispersion relation and time-of-flight patterns for atoms in optical lattice under uniform artificial magnetic field $f = 1/2$ and additional staggering potential $\tilde{\Delta}$ driving particle hopping for $\tilde{\Delta}$ equal to: a) 0, b) 0.1, c) 0.6, d) 1.2, e) 2. The TOF images depict superfluid state (the first column, $V_0/E_R = 5$), system close to the phase transition (the second column, $V_0/E_R = 7.5$) and the Mott insulator (the last column, $V_0/E_R = 10$).

the superfluid – Mott insulator phase transition the mobility of atoms is naturally decreased. Once again, this allows to observe the weak maxima in momentum distribution of incoherent particles which are located around $\mathbf{k} = 0$ regardless of the position of the superfluid phase coherence peaks.

A slightly different behavior can be observed for a system without artificial magnetic field, but with the staggering potential $\tilde{\Delta}$ (see, Fig. 5). Since the flux is missing, the maxima occur at $\mathbf{k} = 0$, however their density in k_x direction is doubled due to increased size of an elementary cell (with the width of the Brillouin zone halved). Increase of $\tilde{\Delta}$ leads to smearing of the peaks in k_x direction. The dispersion relations are quite different: the Dirac cones are not present and the spectrum is gapped for every value of $\tilde{\Delta}$. Also, a noticeable difference occurs for $\tilde{\Delta} \approx 0$: in the system with $f = 0$ the TOF images change discontinuously while going from non-zero to zero value of $\tilde{\Delta}$. This results from the fact that presence of the staggering potential breaks the translational symmetry doubling the size of the elementary cell for every value

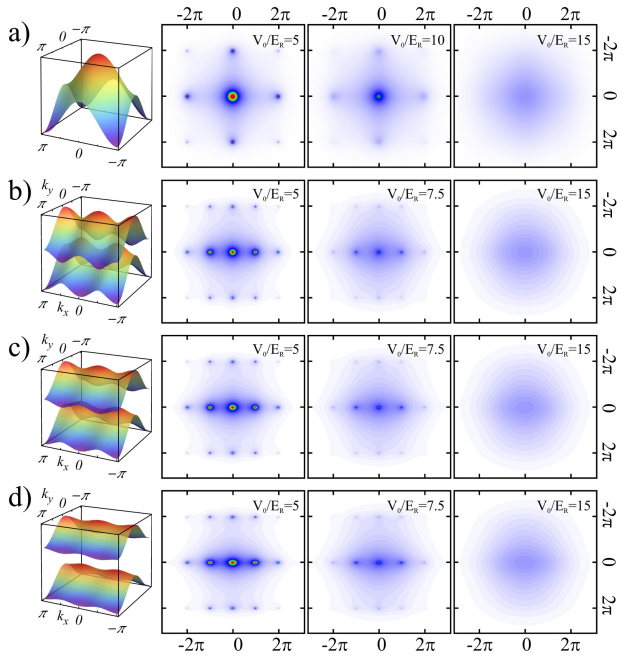

Figure 5: (Color online) Dispersion relation and time-of-flight patterns for atoms in optical lattice under additional staggering potential $\tilde{\Delta}$ driving particle hopping for $\tilde{\Delta}$ equal to: a) 0, b) 0.6, c) 1.2, d) 2. The TOF images depict superfluid state (the first column), system close to the phase transition (the second column) and the Mott insulator (the last column).

of $\tilde{\Delta}$, but not for $\tilde{\Delta} = 0$ (see, differences between Figs. 5a and b-e). This is in contrast to the $f = 1/2$ case, where the enlargement of the elementary cell resulting from the presence of the π flux per plaquette and the staggering potential are the same.

C. Checkerboard staggered flux

A time-independent lattice model with an artificial staggered magnetic field that is used in the present work can effectively describe time-dependent optical lattice with staggered particle current in the tight-binding regime [36]. As a result, it is possible to describe group of experiments that use temporal modification of the optical potential. They allow reaching regimes, where anisotropic Dirac cones emerge in the single-particle spectrum leading to two inequivalent conical points in the energy band, which results in two distinct energy minima that depend on the magnitude of the staggered magnetic flux ϕ. Consequently, it is possible to realize the artificial magnetic field as presented in Fig. 1c, where the flux is staggered and arranged in checkerboard configuration. This method allows to reach values of flux per plaquette ranging from -2π to 2π. The resulting time-of-flight images are presented in Fig. 6. For small fluxes ϕ the effect of the magnetic field is hardly noticeable, as the strong maximum at $\mathbf{k} = 0$ is visible. For $\phi = \pi$ (see Fig.

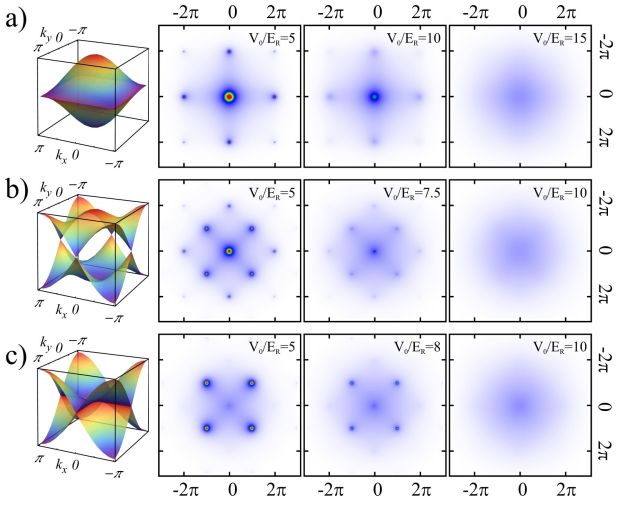

Figure 6: (Color online) Dispersion relation and time-of-flight patterns for atoms in optical lattice in *checkerboard* staggered artificial magnetic field with flux ϕ per plaquette: a) 0, b) π, c) 2π. The TOF images depict superfluid state (the first column), system close to the phase transition (the second column) and the Mott insulator (the last column).

6b)) the energy minima of the two conical points become equal, leading to peaks in momentum distribution located in $\mathbf{k} = 0$ and $\mathbf{k} = (\pm\pi, \pm\pi)$ points. Finally Fig. 6c), for larger fluxes the non-zero momentum state takes over reaching maximum intensity for $\phi = 2\pi$. It should be stressed that in a naive view the impact of the flux $n2\pi$ (n being integer) should be negligible. However, here the $\phi = \pm 2\pi$ flux leads to non-trivial superfluid phase with non-zero momentum. This issue will be discussed in the following subsections.

D. Uniaxially staggered flux

Photon-assisted tunneling in an optical superlattice generating large tunable effective magnetic fields for ultra-cold atoms demonstrated possibility of realization of the large tunable uniaxially staggered field (where the spatial average of the flux is zero) [10]. It was shown that the atomic sample relaxes to the minima of the magnetic band structure, realizing an analogue of a frustrated classical spin system. The obtained time-of-flight patterns for various system hopping anisotropies [10, 35] agree well with the ones calculated with the method presented in the current work (see, Fig. 7). Positions of the maxima of the momentum distribution are correctly recreated as well as the decay of the envelope of the TOF image substantiating choice of the module of the Wannier function in Eq. (20). For isotropic system, the time-of-flight patterns exhibit two minima located around the zero momentum at $\mathbf{k} = \pm(\pi/4, \pi/4)$. While the anisotropy between raw hopping in the x ($t_{i+1,j}$) and y ($t_{i,j+1}$) direction is introduced, for $t_{i+1,j}/t_{i,j+1} \leq \sqrt{2}$, the peaks

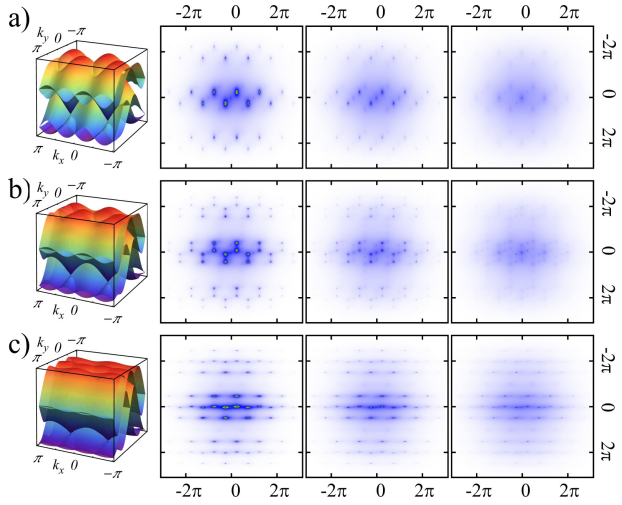

Figure 7: (Color online) Dispersion relation and time-of-flight patterns for atoms in optical lattice in uniaxially staggered artificial magnetic field with flux per plaquette $\phi = \pi/2$ for hopping anisotropy leading ratio of $t_{i+1,j}/t_{i,j+1}$ equal to : a) 1, b) 2, c) 3. The TOF images depict superfluid state (the first column), system close to the phase transition (the second column) and the Mott insulator (the last column).

split into pairs of peaks in agreement with changes of the magnetic band structure.

E. Arbitrary gauge geometry

Although, the flux configuration in the case of the uniaxially staggered flux (see, Sec. IV D and Fig. 1) is pretty regular: uniaxially alternating values of $+\pi/2$ and $-\pi/2$ every second plaquette, the structure of the TOF images is complicated and strongly dependent on the lattice parameters like hopping anisotropy. It results from complex gauge that was used in the experiment in Ref. [10]. However, the same configuration of the flux per plaquette can be obtained for much simpler gauge, as presented in Fig. 8b (the dispersion relation obtained in the same manner as in Ref. [10], however without phase change along k_x direction hopping). The comparison of the resulting time-of-flight patterns is presented in Fig. 9 and it is clearly visible that they are not identical. It can be seen that in case of atoms moving in the tight-binding scheme in the optical lattice the value of the flux being assigned to an elementary cell *does not determine* the momentum distribution of the particles. Other than that, what is crucial is the *change of the quantum phase* that occurs at every bond that the particle travels along, since all the jumps are separated acts rather than a continuous move. This can lead to a non-intuitive situation of particles exhibiting the influence of the vector potential field resulting of a non-zero phase change on selected bonds, although the total phase change on closed trajectory around an elementary cell is zero, which also means that so is the effective flux per plaquette. Such situation

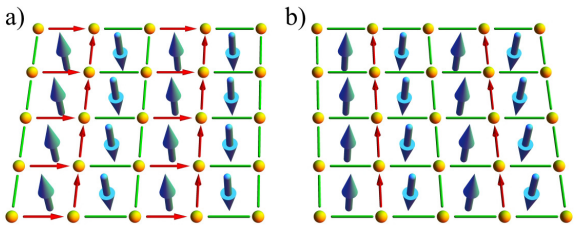

Figure 8: (Color online) Comparison of the gauge used in Ref. [10] and a simpler one resulting in the same configuration of the fluxes (denoted by thick, blue arrows located inside the unit cell) $\pm\pi/2$, while traveling around a plaquette. Thin arrows (red) denote direction of hopping along which a particle phase changes by $\pi/2$ ($-\pi/2$ in an opposite direction), while tubes (green) represent regular hopping with no phase change.

is presented in Fig. 10: the configuration of the gauge results in change of phase equal to zero when a particle travels around a closed loop. However, the resulting time-of-flight patterns are still dependent on the phase ϕ acquired during a single jump leading to dispersion relation:

$$t(\mathbf{k}) = t\left[\cos(k_x + \phi) + \cos(k_y + \phi)\right]. \tag{21}$$

For free condensate (without optical lattice) the superfluid velocity:

$$\mathbf{v}_s = \frac{\hbar}{m}\nabla\phi. \tag{22}$$

The kinetic energy E_k can be expanded around its minimum at $\mathbf{k}_\phi = (-\phi, -\phi)$, which leads to $\mathbf{v}_s \sim \partial E_k/\partial k = \hbar\mathbf{k}_\phi/m$. As a result, change of the particles momentum resulting from phase acquired on a jump along a single bond is simply:

$$k \sim \nabla\phi, \tag{23}$$

which is consistent with the results in Fig. 10. It is worth to notice that using such simple gauge configuration one obtains a finite momentum superfluid phase with the non-zero phase change imposed on the condensate wave function but with the zero value of the artificial magnetic field.

V. SUMMARY

In conclusion, we have analyzed the correlations between strongly interacting bosons confined in two-dimensional square lattice in the presence of an artificial magnetic field using quantum rotor model that is inherently combined with the Bogolyubov approach. The flexibility of the method and its sensitivity to the spatial fluctuations allows us to consider various geometries of the magnetic flux (uniform, checkerboard, uniaxially staggered), which are expected to be realizable,

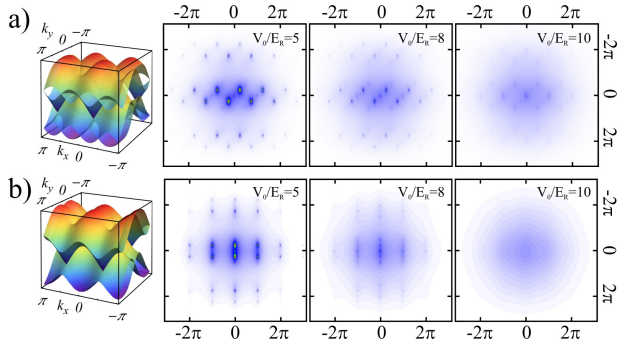

Figure 9: (Color online) Comparison dispersion relation and time-of-flight patterns for atoms in optical lattice in different gauges (see, Fig. 8), which lead to the same uniaxially staggered configuration of the magnetic flux.

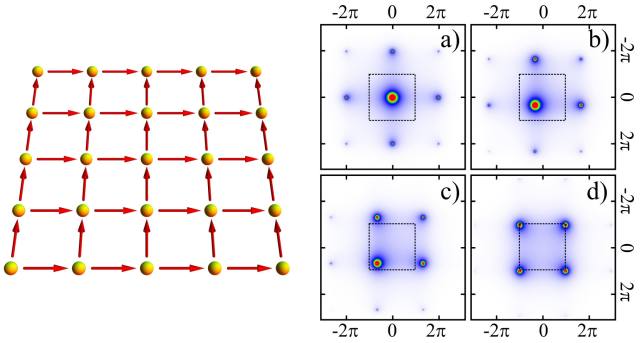

Figure 10: (Color online) Gauge resulting in zero flux (red arrows denote direction of hopping along which a particle phase changes by ϕ) and resulting time-of-flight patterns for atoms in optical lattice for $V_0/E_R = 7.5$ and a) $\phi = 0$, b), $\phi = \pi/3$, c) $\phi = 2\pi/3$ and d) $\phi = \pi$. Dotted boxes mark the first Brillouin zone.

or have already been implemented in experimental settings. Furthermore, we have calculated the time-of-flight patterns, which give information about dynamics of condensed atoms surrendered to the artificial magnetic field. We validate our approach by successfully recreating experimentally observed TOF images and recovering the superfluid-Mott insulator phase transition, which is driven by the interactions. Also, we show in which conditions novel superfluid phases with non-zero momentum can arise leading to observation of Dirac-like physics in optical lattices. Furthermore, we deduce that the crucial element for a proper recreation of the time-of flight patterns is not the flux configuration but rather the change of the quantum phase that occurs at every bond described by the dispersion relation and consequently the density of states. Thus, the TOF images result directly from the chosen and experimentally realized gauge. This is in clear contrast with solid state physics, where attainable values of flux per elementary cell are very small (flux $f = 1/2$ would require fields of the order of $10^2 - 10^3$T). As a result, the spatial change of the vector potential (gauge) is very gradual and the phase acquired by particles on a single hop is marginal. However, in optical lattices, the attainable values of the flux are very high and the phase change on single bonds can be individually controlled. This leads to the strong dependence of the time-of-flight patterns and the atom dynamics on the specific gauge configuration rather then the resulting magnetic flux. Therefore, in systems of strongly interacting bosons, only the minima of the kinetic energy (maxima of the dispersion relation in the k-space) determine the superfluid properties of the ultra-cold atoms confined in optical lattices. At the same time, the interactions between atoms change the phase stiffness and the density of the condensate rather than the dynamical properties of the coherent particles.

Acknowledgments

T.P.P. would like to thank for the hospitality of I. Bloch's group at MPQ in Garching and many fruitful discussions concerning experiments with bosonic species, especially with M. Aidelsburger and the *Bosons*. T.P.P. would like to acknowledge partial funds from the Human Capital Operational Programme, Grant No. UDA-POKL.04.01.01-00-133/09-00. We would also thank M. Aidelsburger for insightful and helpful comments regarding the manuscript.

VI. APPENDIX

Quasiparticle spectrum and the density of states

In the following, we present dispersion relations and the resulting lattice densities of states for various flux geometries, which were described in Sec. IV.

1. *Staggered potential with uniform flux f=0 for two-dimensional square lattice*

The dispersion relation contains two sub-bands [34]

$$t_0(\boldsymbol{k}) = 2t\left(\cos k_y \pm \sqrt{\cos^2 k_x + \Delta^2}\right) \tag{24}$$

and results from the single-particle Schrödinger equation:

$$\begin{aligned} E\psi_{m,n} &= -t\psi_{m,n+1} - t\psi_{m,n-1} - t\psi_{m+1,n} \\ &\quad -t\psi_{m-1,n} + (-1)^m \Delta\psi_{m,n}, \end{aligned} \tag{25}$$

which allows to deduce hopping elements t_{mn} (m, n number the lattice sites in x and y directions, E is the energy and ψ – the wave function) between neighboring sites. The density of states is given by a nonlinear convolution:

$$\begin{aligned} \rho_0(E,\Delta) &= \frac{1}{2\pi^2 t}\int dx \rho_{1D}(x) \\ &\quad \times \rho_{1D}\left(\frac{E}{2t} \pm \sqrt{x^2+\Delta^2}\right), \end{aligned} \tag{26}$$

where $\rho_{1D}(x)$ is a one-dimensional lattice density of states:

$$\rho_{1D}(E) = \frac{1}{2\pi^2}\frac{1}{\sqrt{1-\left(\frac{E}{2t}\right)^2}} \tag{27}$$

resulting from $t(\boldsymbol{k}) = 2t\cos k_x$ dispersion relation.

2. Staggered potential with uniform flux f=1/2 for the two-dimensional square lattice

The dispersion relation [34]:

$$\left|t_{1/2}(\boldsymbol{k})\right| = 2t\sqrt{\cos^2 k_x + (\cos k_y - \Delta)^2} \tag{28}$$

for $\Delta = 0$ is equal to the uniform external magnetic field with $f = 1/2$. It results from the Schrödinger equation:

$$\begin{aligned} E\psi_{m,n} &= -t\psi_{m,n+1}e^{i\pi m} - t\psi_{m,n-1}e^{-i\pi m} \\ &- t\psi_{m+1,n} - t\psi_{m-1,n} + (-1)^m\Delta\psi_{m,n}. \end{aligned} \tag{29}$$

The resulting DOS reads:

$$\begin{aligned} \rho_{1/2}(E,\Delta) &= \frac{|E|}{2\pi^2 t}\int dx \frac{\rho_{1D}(x)}{\sqrt{\left(\frac{E}{2t}\right)^2 - (x-\Delta)^2}} \\ &\times \rho_{1D}\left(\sqrt{\left(\frac{E}{2t}\right)^2 - (x-\Delta)^2}\right). \end{aligned} \tag{30}$$

3. Checkerboard staggered flux for the two-dimensional square lattice

The dispersion relation for the flux ϕ is given by the formula [36]:

$$\begin{aligned} |t_\phi(\boldsymbol{k})| &= 2t\left[2\cos\left(\frac{\phi}{2}\right)\cos\left(\frac{k_x+k_y}{2}\right)\cos\left(\frac{k_x-k_y}{2}\right)\right. \\ &+ \left.\cos^2\left(\frac{k_x+k_y}{2}\right) + \cos^2\left(\frac{k_x-k_y}{2}\right)\right]^{1/2} \end{aligned} \tag{31}$$

and results from the Schrödinger equation:

$$\begin{aligned} E\psi_{m,n} &= -t\psi_{m,n+1}e^{i(-1)^p\frac{\phi}{4}} - t\psi_{m,n-1}e^{-i(-1)^p\frac{\phi}{4}} \\ &- t\psi_{m+1,n}e^{-i(-1)^p\frac{\phi}{4}} - t\psi_{m-1,n}e^{i(-1)^p\frac{\phi}{4}} \end{aligned} \tag{32}$$

with $p = m + n$. The DOS can be written in the form:

$$\begin{aligned} \rho(E,\phi) &= \frac{|E|}{2\pi^2 t}\int \frac{dx}{\cos\frac{\phi}{2}+x}\rho_{1D}(x) \\ &\times \rho_{1D}\left(\frac{E^2+x^2-1}{\cos\frac{\phi}{2}+x} - x\right) \end{aligned} \tag{33}$$

where any value of flux ϕ is allowed.

4. Uniaxially staggered flux

The dispersion relation for gauge configuration used in experiments presented in Ref. [10] consists of four subbands:

$$\begin{aligned} t_{1,2}(\mathbf{k}) &= \sin k_x - \eta\cos k_y \\ &\pm \sqrt{\eta^2 - 2\sin 2k_x + \eta^2\sin 2k_y + 2} \\ t_{3,4}(\mathbf{k}) &= t_{1,2}\left[\mathbf{k} - \left(\frac{\pi}{2},\frac{\pi}{2}\right)\right], \end{aligned} \tag{34}$$

where η is a hoping anisotropy ratio, while the dispersion used in Fig. 8b, reads:

$$\begin{aligned} t_{1,2}(\mathbf{k}) &= \cos k_y - \sin k_y - \sqrt{2\cos 2k_x + \sin 2k_y + 3} \\ t_{3,4}(\mathbf{k}) &= t_{1,2}\left[\mathbf{k} - \left(\frac{\pi}{2},0\right)\right]. \end{aligned} \tag{35}$$

In both cases, analytical formulas for the lattice density of states cannot be easily obtained. The details of calculation of the dispersion in Eq. (34) can be found in Ref. [10].

[1] M. H. Anderson, J. R. Ensher, M. R. Matthews, C. E. Wieman, and E. A. Cornell Science, **269**, 198 (1995).
[2] M. Greiner, O. Mandel, T. W. Hänsch and I. Bloch, Nature **415**, 39 (2002).
[3] D. Jaksch, C. Bruder, J. I. Cirac, C. W. Gardiner, and P. Zoller, Phys. Rev. Lett. **81**, 3108 (1998).
[4] A. Leggett, *Quantum liquids* (Oxford, New York, 2006).
[5] N. R. Cooper, Adv. Phys. **57**, 539 (2008).
[6] D. Jaksch and P. Zoller, New J. Phys. **5**, 56 (2003).
[7] F. Gerbier and J. Dalibard, New J. Phys. **12**, 033007 (2010).
[8] A. Kolovsky, Europhys. Lett. **93**, 20003 (2011).
[9] Y.-J. Lin, R. L. Compton, K. Jiménez-García, J. V. Porto and I. B. Spielman, Nature, **462**, 628 (2009).
[10] M. Aidelsburger, M. Atala, S. Nascimbène, S. Trotzky, Y.-A. Chen, and I. Bloch, Phys. Rev. Lett. **107**, 255301 (2011); M. Aidelsburger, M. Atala, S. Nascimbène, S. Trotzky, Y.-A. Chen, I. Bloch, arXiv:1212.2911.
[11] K. Osterloh, M. Baig, L. Santos, P. Zoller, and M. Lewenstein, Phys. Rev. Lett. **95**, 010403 (2005).
[12] P. Hauke, O. Tieleman, A. Celi, C. Ölschläger, J. Simonet, J. Struck, M. Weinberg, P. Windpassinger, K.

Sengstock, M. Lewenstein and A. Eckardt, Phys. Rev. Lett. **109**, 145301 (2012).
[13] P. Harper, Proc. Phys. Soc. London Sect. A **68**, 874 (1955).
[14] D. Hofstadter, Phys. Rev. B **14**, 2239 (1976).
[15] T. A. Zaleski and T. K. Kopeć, Phys. Rev. A **84**, 053613 (2011).
[16] T. A. Zaleski, Phys. Rev. A **85**, 043611 (2012); T. A. Zaleski, J. Phys. B: At. Mol. Opt. Phys. **45**, 145303 (2012).
[17] T. P. Polak and T. K. Kopeć, Phys. Rev. **A** 79, 063629 (2009).
[18] S. Sinha and K. Sengupta, Eur. Phys. Lett. **93**, 30005 (2011).
[19] T. P. Polak and T. K. Kopeć, Phys. Rev. B **76**, 094503 (2007).
[20] T. P. Polak and T. K. Kopeć, J. Phys. B: At. Mol. Opt. Phys. **42,** 095302 (2009).
[21] T. A. Zaleski, T. P. Polak, Phys. Rev. A **83**, 023607 (2011); T. P. Polak, T. A. Zaleski, Acta. Phys. Pol. A **121**, 1312 (2012).
[22] B. Capogrosso-Sansone, Ş. Güneş Söyler, Nikolay Prokof'ev and B. Svistunov, Phys. Rev. A **77**, 015602 (2008).
[23] N. Teichmann, D. Hinrichs, M. Holthaus, and A. Eckardt, Phys. Rev. B **79**, 100503 (2009).
[24] M. Ö. Oktel, M. Niţă, and B. Tanatar, Phys. Rev. B **75**, 045133 (2007).
[25] M. Niemeyer, J. K. Freericks, and H. Monien, Phys. Rev. B **60**, 2357 (1999).
[26] P. B. Blakie and C. W. Clark, J. Phys. B: At. Mol. Opt. Phys. **37**, 1391, (2004).
[27] T. Vojta, Phys. Rev. **B** 53, 710 (1996).
[28] Y. Kato, Q. Zhou, N. Kawashima and N. Trivedi, Nature Physics **4**, 617 (2008).
[29] S. Powell, R. Barnett, R. Sensarma, and S. Das Sarma, Phys. Rev. Lett. **104**, 255303 (2010); S. Powell, R. Barnett, R. Sensarma, and S. Das Sarma, Phys. Rev. A **83**, 013612 (2011).
[30] L. Pollet, N. V. Prokof'ev, and B. V. Svistunov, Phys. Rev. Lett. **104**, 245705 (2010).
[31] M. Aidelsburger and *Bosons,* private communication.
[32] J. Hecker Denschlag, J. E. Simsarian, H. Häffner, C. McKenzie, A. Browaeys, D. Cho, K. Helmerson, S. L. Rolston and W. D. Phillips, J. Phys. B: At. Mol. Opt. Phys. **35**, 3095 (2002).
[33] L. Fallani, F. S. Cataliotti, J. Catani, C. Fort, M. Modugno, M. Zawada, and M. Inguscio, Phys. Rev. Lett. **91**, 240405 (2003).
[34] P. Delplace and G. Montambaux, Phys. Rev. B **82**, 035438 (2010).
[35] G. Möller and N. R. Cooper, Phys. Rev. A **82**, 063625 (2010).
[36] Lih-King Lim, C. Morais Smith, A. Hemmerich, Phys. Rev. Lett. **100**, 130402 (2008); Lih-King Lim, A. Hemmerich, and C. Morais Smith, Phys. Rev. A **81**, 023404 (2010).